Effective properties of superstructured hyperbolic metamaterials: How to beat the diffraction limit at large focal distance

Emmanuel Centeno[*] and Antoine Moreau

Clermont Université–Université Blaise Pascal, Institut Pascal, Boîte Postale 10448, F-63000 Clermont-Ferrand, France
and CNRS, UMR 6602, Institut Pascal, F-63177 Aubière, France

Superstructured hyperbolic metamaterials (HMs) have been recently introduced to realize media with effective index -1 with the ultimate goal of designing flat lenses of super-resolution power for optical imaging applications. In this work, we analyze the impact on their effective optical properties of defect metallic layers periodically added in HMs. The effective index and losses are systematically calculated in both homogenization and diffractive regimes and with respect to the ratio of dielectric and metallic layers. Although the superstructuring can dramatically decrease the effective losses, we demonstrate that the extent of the hyperbolic dispersion curve in k space plays an even more fundamental role for breaking the diffraction limit. Optimized superstructured HMs working in a regime between the homogenization and diffractive regimes are shown to present simultaneously low effective losses and a high optical resolution for visible light. These superstructured HMs present an effective index of -5 and extend the subwavelength focalization distance up to 2λ, which is twice as large as for regular HMs.

PACS number(s): 42.25.−p, 78.67.Pt, 42.25.Fx, 78.20.Ci

I. INTRODUCTION

Hyperbolic metamaterials (HMs) are artificial anisotropic materials characterized by effective permittivity or permeability tensors presenting positive and negative principal components [1]. This property allows expansion of the classical electromagnetic materials' frontiers and opens attractive routes for the design of novel photonic systems [2,3]. Hyperbolic metamaterials have, for example, been shown to reduce the Purcell factor [4–6], to enhance the optical absorption [7–10], or to break the thermodynamic radiation limits [11,12]. These effects are essentially related to the particular dispersion relation of photons, which is characterized by a hyperboloid shape in the wave vector space. As a consequence, the whole spectrum of evanescent waves emitted by a given source is converted into propagating waves inside HMs. This canalization mechanism, associated with a negative refraction phenomenon, leads to the concept of flat lenses that can break the diffraction limit [13–17]. Several results demonstrate the efficiency of this canalization regime in the microwave regime where metallic losses are weak [18–20]. This ability of flat lenses made of metal-dielectric multilayers to form super-resolved images has been theoretically studied, and a lens equation has been established to determine the focal distance [21,22]. A superstructuring of the multilayer has also been proposed for realizing HMs of -1 effective index [23]. These superstructured HMs made of Ag-TiO$_2$ layers have been experimentally studied for ultraviolet light, and an all-angle negative refraction has been demonstrated [24]. However, according to the authors, super-resolution was not reached because of the optical losses due to the metallic absorption. In this framework, it could seem surprising to define an effective index for HMs, since they are intrinsically anisotropic materials. This contradiction was lifted in [21], where the calculation of this optical effective index was done by a direct derivation from the curvature of the hyperbolic dispersion.

This approach leads to an analytical expression of the effective optical index in terms of the effective permittivity tensor components in the long-wavelength limit. In the diffractive regime, this effective index is retrieved by the numerical calculation of the curvature of the dispersion curve in k space. Guided by this theory, HMs of -5 effective index have been shown to produce subwavelength images for visible light when the focal distance is smaller than the wavelength. The superstructuring of hyperbolic metamaterials has also led to the concept of hypercrystals, which makes a link between the metamaterial and photonic-crystal approaches [25]. Hypercrystals are characterized by a scale of the superstructuring very large compared to that of hyperbolic metamaterials. In this regime, hypercrystals sustain surface states of long propagation distances that may have an important impact on super-resolution.

The aim of this work is to study the effective properties of superstructured HMs that consist of a set of metallic defect layers introduced at a scale close to that of the HM period. Particular attention is paid to the evaluation of the optical resolution of flat lenses based on superstructured HMs that present an effective index of -1 as in the experiment of Xu *et al.* [24]. We found that the superstructuring lowers the effective losses, which favors the focalization of subwavelength images. This result is, however, tempered by a detailed analysis of the hyperbolic dispersion. We demonstrate that the spatial extension of the dispersion curve in k space plays a crucial role for beating the diffraction limit. By studying the maximal optical resolution, which derives from a cutoff for the transverse wave vector, we demonstrate that superstructured HMs working in the diffractive regime as in the experiment of Xu *et al.* [24] cannot surpass Abbe's limit. We show nevertheless that metallic defects actually enhance the optical properties of HMs between the homogenization and diffractive regimes. This systematic study of superstructured HMs leads to the design of a flat lens able to focus subwavelength images in the visible spectrum of light and for large focal distances up to 2λ.

---

[*]Corresponding author: emmanuel.centeno@univ-bpclermont.fr

The present article begins with essential definitions for calculating the complex effective index, and the homogenization and diffractive regimes are defined. Section III analyzes the impact of the metallic defects on the effective properties in the homogenization regime. Section IV extends this study to the diffractive regime, where resonant behaviors are found for the effective index and the associated effective losses with respect to the wavelength and the size of the defect layers. In Sec. V, we demonstrate that the spatial extension of the hyperbolic dispersion in k space is a crucial parameter to consider for obtaining a high optical resolution. In Sec. VI, we consider a regime between the homogenization and diffractive regimes which allows us to find a compromise design that supports moderate effective losses and a high optical resolution. These superstructured HMs are shown to beat the diffraction limit for focal distances up to two wavelengths.

II. OPTICAL EFFECTIVE PARAMETERS FOR HYPERBOLIC METAMATERIALS

Hyperbolic metamaterials consist of a periodic set of stacked metal (M) and dielectric (D) layers with respective thicknesses and permittivities ($h_m, \bar{\epsilon}_m$) and ($h_d, \bar{\epsilon}_d$). The lattice period of the multilayer is defined by $D = h_m + h_d$ and the filling factors in metal and dielectric are respectively $f_m = h_m/d$ and $f_d = h_d/d$. We consider silver and TiO$_2$ layers as in [24]. The permittivities considered here are both complex since the optical absorption cannot be neglected at optical frequencies [26]. Metals present a permittivity with a negative real part, whereas dielectrics have a permittivity with a positive real part. For p-polarized light and in the long-wavelength limit ($\lambda \gg D$) the (MD) multilayer is equivalent to an anisotropic medium whose effective permittivity principal elements are [14,27]

$$\bar{\epsilon}_x = \bar{\epsilon}_m f_m + \bar{\epsilon}_d f_d, \quad \bar{\epsilon}_y = \left(\frac{f_m}{\bar{\epsilon}_m} + \frac{f_d}{\bar{\epsilon}_d} \right)^{-1}. \quad (1)$$
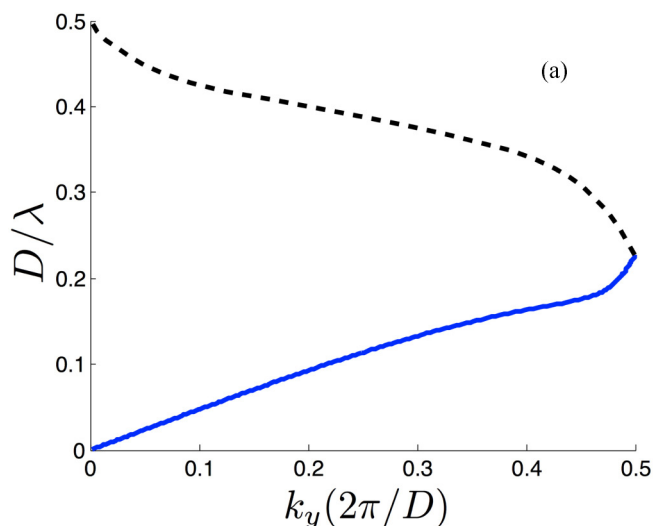
With an appropriate choice of the metal filling factor, opposite signs for the real parts of the effective components can be obtained, $\epsilon_x > 0$ and $\epsilon_y < 0$, so that the (MD) multilayer presents a hyperbolic dispersion relationship:

$$k_x^2/\bar{\epsilon}_y + \bar{k}_y^2/\bar{\epsilon}_x = (\omega/c)^2. \quad (2)$$

Note that the homogenization procedure that allows this effective dispersion relation to be derived is based on two assumptions: the quasistatic limit ($\lambda \gg D$) and small transverse wave vectors ($k_x \ll k_0$) [27]. This latter condition has been proved to be crucial in several studies [28–31]. We have recently demonstrated that an effective complex index can be extracted from the previous dispersion relation [21]. This refractive index is related to the curvature of the isofrequency curves (IFCs) and can be introduced by approximating the photonic dispersion by the following parabolic expression:

$$\bar{k}_y(k_x) = \bar{k}_y(0) - \bar{\gamma} k_x^2/2k_0, \quad (3)$$

where the complex curvature $\bar{\gamma} = -k_0(\partial^2 \bar{k}_y/\partial k_x^2)|_{k_x=0}$. The effective index is introduced by identifying the curvature of a HM with that of a homogeneous medium. With this definition the complex effective index $\bar{n} = n + i\kappa$ is linked to the complex curvature by

$$n = 1/\mathrm{Re}(\bar{\gamma}) \quad (4)$$

and

$$\kappa = |\mathrm{Im}(\bar{\gamma})/\mathrm{Re}(\bar{\gamma})|. \quad (5)$$

The calculation of the complex effective index allows a systematic optimization of hyperbolic metamaterials. In particular, the effective losses are determined with the figure of merit (FOM) defined by $\mathcal{F} = |n/\kappa|$ that helps in the design of efficient flat lenses [21]. Here, we want to specify the validity domain of the homogenized regime. Figure 1 represents the dispersion diagram for an (MD) multilayer and three isofrequency curves (IFCs) calculated with the exact dispersion relation given in [27]. We found a good agreement
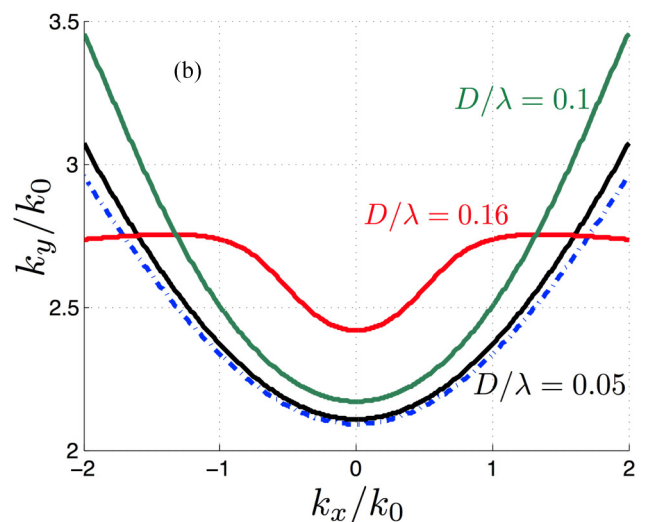
FIG. 1. (Color online) (a) Dispersion diagram for an (MD) multilayer computed at $\lambda = 350$ nm and for $h_m/h_d = 1$. The solid and dashed curves are respectively the first and second Bloch bands. (b) Isofrequency curves calculated from three reduced frequencies D/λ. The dashed blue curve is obtained from the homogenized dispersion relation given by Eq. (2).
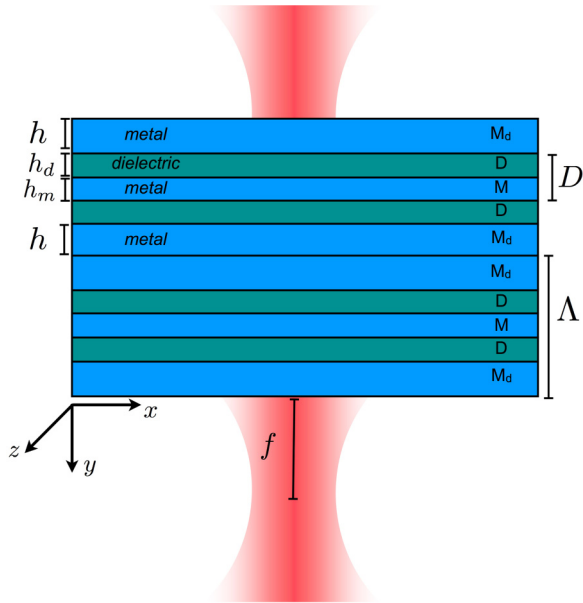
FIG. 2. (Color online) Superstructured hyperbolic metamaterial characterized by a supercell $(M_d D M D M_d)$.

with the ICF calculated with the analytical expression of Eq. (2) [dotted line on Fig. 2(b)] for reduced frequencies D/λ smaller than 0.05 (and for $k_x < 2k_0$). In practice it amounts to realizing thin metal and dielectric layers of thicknesses about 10 nm at $\lambda = 340$ nm. For higher reduced frequencies the exact IFCs cannot be reproduced by the homogenization approach even for lattice periods D as small as 0.16λ. On the contrary, a very great variation of the curvature of the IFCs is observed as the reduced frequency approaches the top of the first band around $D/\lambda = 0.2$. This results led us to distinguish three main regimes: the homogenization regime for $D/\lambda < 0.05$ where the effective permittivities given in Eq. (1) are valid; the diffractive regime for $D/\lambda > 0.14$ where the lattice period drastically modifies the dispersion of light; and a regime in between for $0.05 < D/\lambda < 0.14$ with an anisotropy similar to that observed for the homogenization regime but with effective properties that cannot be derived from the analytical formulas of Eq. (1). The next section is devoted to the study of the effective properties of superstructured hyperbolic metamaterials operating in the homogenization regime.

III. STUDY OF THE COMPLEX EFFECTIVE INDEX IN THE HOMOGENIZATION REGIME

In this section, we first demonstrate that the hyperbolic feature of the metal-dielectric multilayer is conserved in the homogenization regime when an additional metallic defect layer is periodically introduced. Second, we show that the effective index can be tuned by varying the thickness of the defect layer denoted (M_d). For that purpose, we consider the superstructured hyperbolic metamaterial depicted on Fig. 2. The supercell is described by the following sequence: $(M_d D M D M_d)$ where the defect layer (M_d) is composed of the same metal (Ag) of permittivity $\bar{\epsilon}_m$ but has a different thickness h. To study the impact of this metallic defect, we

choose $h = h_m(1 + \tau)/2$ where $\tau = (2h - h_m)/h_m$ represents the variation of the (M_d) thickness from that of the regular layer (M). The superperiod of the multilayer is given by $\Lambda = 2D + \tau h_m$. To demonstrate that the hyperbolic characteristic of the metamaterial is preserved, the effective permittivities $(\bar{\epsilon}_x^s, \bar{\epsilon}_y^s)$ for the superstructured HM are expressed in terms of those of the (MD) structure:

$$\bar{\epsilon}_x^s = (\bar{\epsilon}_x + \rho\bar{\epsilon}_m)/(1 + \rho),$$
$$1/\bar{\epsilon}_y^s = (1/\bar{\epsilon}_y + \rho/\bar{\epsilon}_m)/(1 + \rho), \tag{6}$$

where $\rho = \tau f_m/2$. For example, the modification of the effective properties induced by the defect (M_d) is plotted on Fig. 3 for $f_m = f_d$ and at $\lambda = 350$ nm. When the thickness of (M_d) increases, i.e., when $\rho > 0$ (and $\tau > 0$), the real part of ϵ_x^s decreases while that of ϵ_y^s increases. As a consequence, the superstructured HM conserves its original hyperbolic properties since the signs of the principal values of the effective permittivity tensor remain unchanged. Moreover, a large variation of the defect layer thickness is required to noticeably modify the effective permittivities. These variations however have a significant impact for beam shaping operations even in the homogenization regime. This effect is caught by the complex effective index calculated with Eqs. (4) and (5) where the complex curvature for the superstructured HM is given by

$$\bar{\gamma}^s = \frac{\sqrt{\bar{\epsilon}^s{}_x}}{\bar{\epsilon}^s{}_y}. \tag{7}$$

A global picture of the impact of the (M_d) layer on the effective index and the figure of merit $\mathcal{F} = |n/\kappa|$ is shown in Fig. 4 where these parameters are plotted as functions of the wavelength, the metal-dielectric ratio, and for three values of τ. The effective index is mostly affected by (M_d) for low metal-dielectric ratio h_m/h_d or for wavelengths higher than 360 nm. For h_m/h_d ranging between 0.5 and 1, the effective index increases when a supplementary fraction of metal is added in the HM. The maximal FOM remains constant at about 3 and shifts to a lower metal-dielectric ratio as τ increases with a constant wavelength centered around 390 nm. Finally, in the long-wavelength regime, the modification brought by the introduction of the defect metallic layer is real, but weak. Actually, the optimal operating regime in terms of maximal FOM $\mathcal{F}$ always corresponds to the same effective index of about -5 whatever the thickness of the defect layer. We also remark that effective indices around -1.5 arise for $\mathcal{F}$ smaller than 1, indicating that these conditions are not suitable for realizing an efficient lens. Since in this homogenization regime the FOM is not enhanced by the additional defect layers, we conclude that the optical resolution of a flat lens based on superstructured HMs is not improved compared to the simplest (MD) multilayers. Let us now analyze the impact of such metallic defects in the diffractive regime.

IV. STUDY OF THE COMPLEX EFFECTIVE INDEX IN THE DIFFRACTIVE REGIME

In the diffractive regime the photonic dispersion strongly depends on the interaction of photons with the periodic lattice. This leads to a dramatic modification of the effective
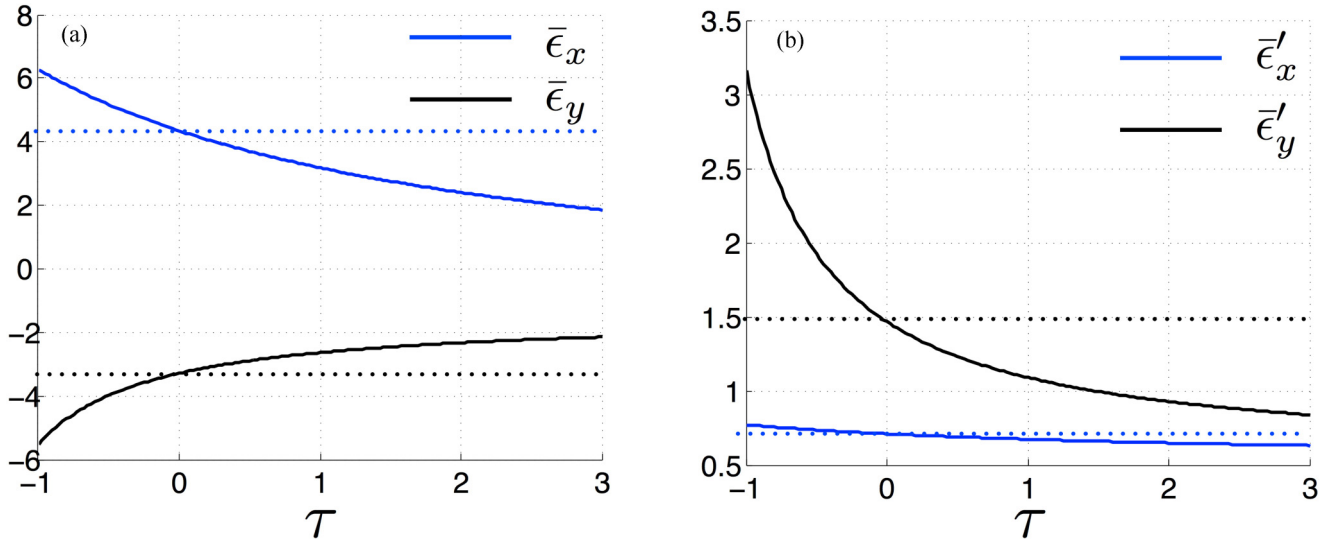
FIG. 3. (Color online) (a) and (b) represent respectively the real and imaginary parts of the effective permittivities $\bar{\epsilon}_x$ and $\bar{\epsilon}_y$ calculated with Eq. (6) as functions of the thickness of the defect layer. Dotted lines show the effective permittivities for the (MD) structure.

properties of HMs when the reduced frequency is set at about $D/\lambda = 0.16$ [21]. In this section, we present the method for computing the complex curvature and the related complex effective index for superstructured HMs. Then we analyze the modification of $\mathcal{F}$ when the thickness of the defect layer varies.

Since the effective permittivities cannot be derived in this resonant regime, the complex wave vector $\bar{k}_y$ has to be numerically calculated from the complex band diagram. For that purpose, the transfer matrix $\bar{T}$ of the supercell depicted in Fig. 2 is computed and the Bloch wave vector is then
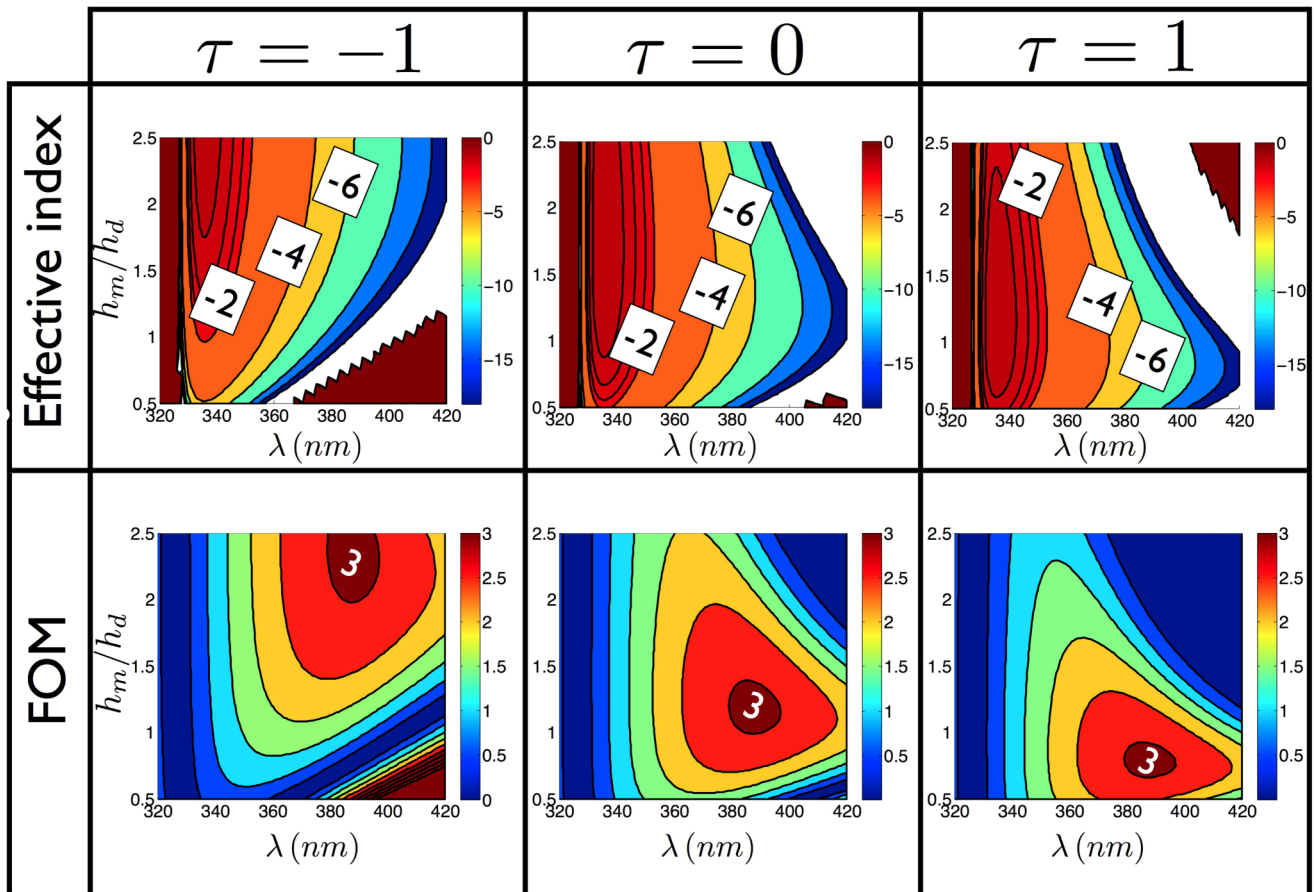
FIG. 4. (Color online) Maps of the effective index and FOM, for three values of τ, with respect to the metal-dielectric ratio (h_m/h_d) and the wavelength. These results are obtained in the homogenization regime by applying Eqs. (4) and (5) with Eq. (7).
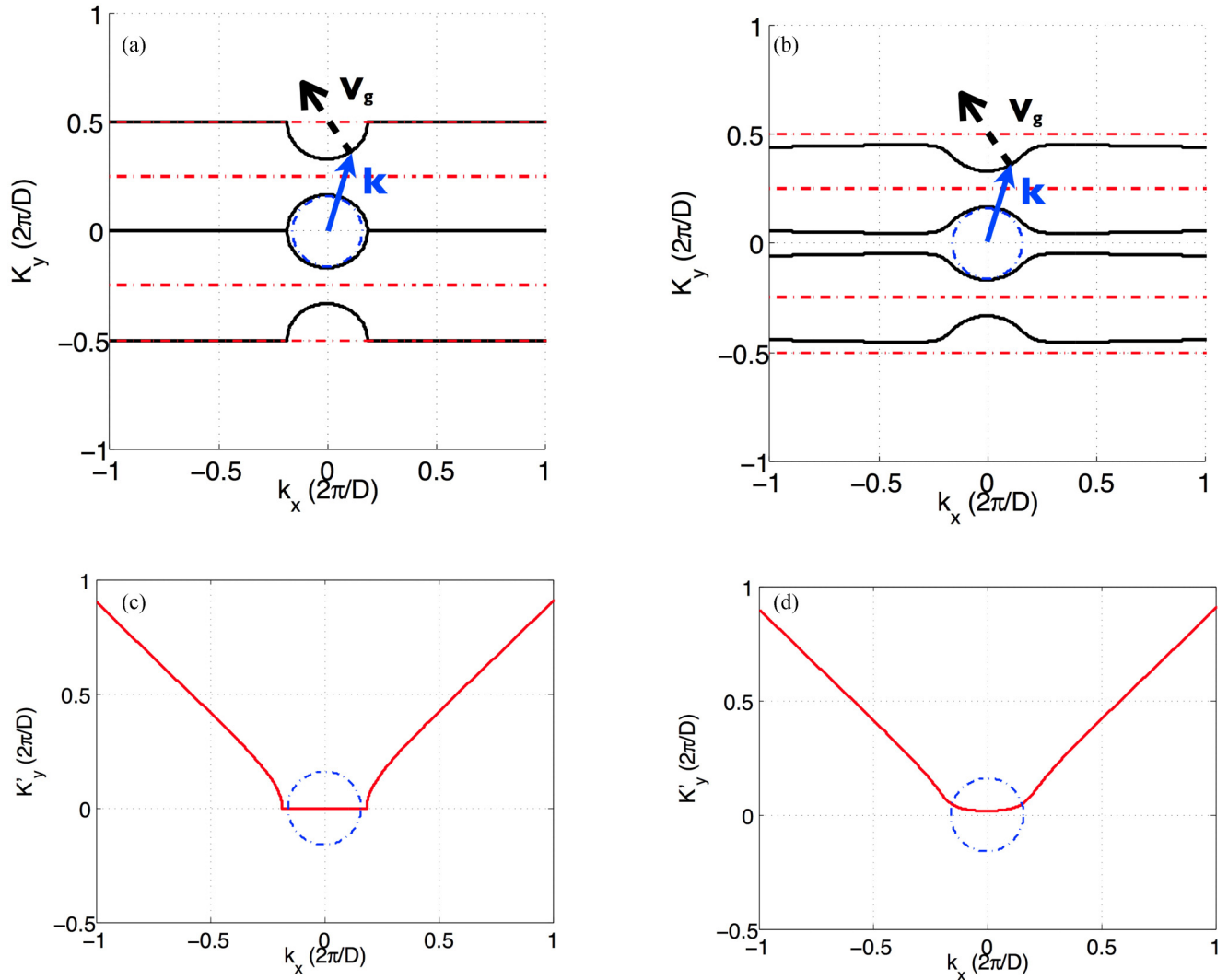
FIG. 5. (Color online) (a),(b) Isofrequency curves computed for $\lambda = 358$ nm, $h_m/h_d = 1.1$, and $\tau = 0$. (a) and (b) are respectively obtained without and with material absorption. The dotted blue circle represents the air IFC. Solid and dashed arrows represent the wave vector and the group velocity. In (c) and (d) are plotted the imaginary part of K_y without and with material absorption, respectively.

obtained by applying $\bar{k}_y = \arccos[\mathrm{tr}(\bar{T})]$ where $\mathrm{tr}(\bar{T})$ designates the trace of the matrix $\bar{T}$. The numerical computation of the isofrequency curves allows calculation of the complex curvature and the complex effective index by applying the definitions of Eqs. (4) and (5).

To understand the effect of the band folding introduced by the superstructuring, the isofrequency curves are plotted in the first Brillouin zone $(-\pi/2D, \pi/2D)$ of the superstructured $(M_d D M D M_d)$ sequence which presents a double lattice period $\Gamma = 2D$. Figures 5(a) and 5(b) are respectively obtained without any optical losses and when the material absorption is taken into account. Moreover, we choose $\tau = 0$ in order to compare this band diagram to that of the (MD) sequence. In the first Brillouin zone of the superstructured HM, these ICFs almost match the air IFC (dotted blue circle) indicating that the effective index is close to -1. We also observe that the ICFs present a limited extension for transverse wave vectors k_x in the approximate range $[-k_0, k_0]$. Beyond this domain the IFCs flatten and correspond to

nonpropagative Bloch modes since the imaginary part of K_y grows rapidly [Figs. 5(c) and 5(d)]. As the reduced frequency approaches the upper limit of the first dispersion band (Fig. 1), the extent of the IFCs diminishes and the curvature decreases. Since for $\tau = 0$ the $(M_d D M D M_d)$ and (MD) sequences are equivalent, we also represent the IFCs in the first Brillouin zone $(-\pi/D, \pi/D)$ of the (MD) multilayer [Figs. 5(a) and 5(b)]. Applying Eq. (4) to these IFCs leads again to a -1 effective index. This analysis leads to the conclusion that in order to apply correctly the definition of the curvature index given in Eqs. (4) and (5), the complex curvature $\bar{\gamma}$ has to be computed in the second Brillouin zone of the superstructured lattice. This principle, well known for photonic crystals, allows any confusion about the optical mechanisms at work to be avoided. This band folding effect has also been evidenced in [32] where the role of the Bloch mode of the second Brillouin zone for the superstructured HM have been highlighted. In the unfolded band structure, it appears that no left-handed properties can be associated with these HMs
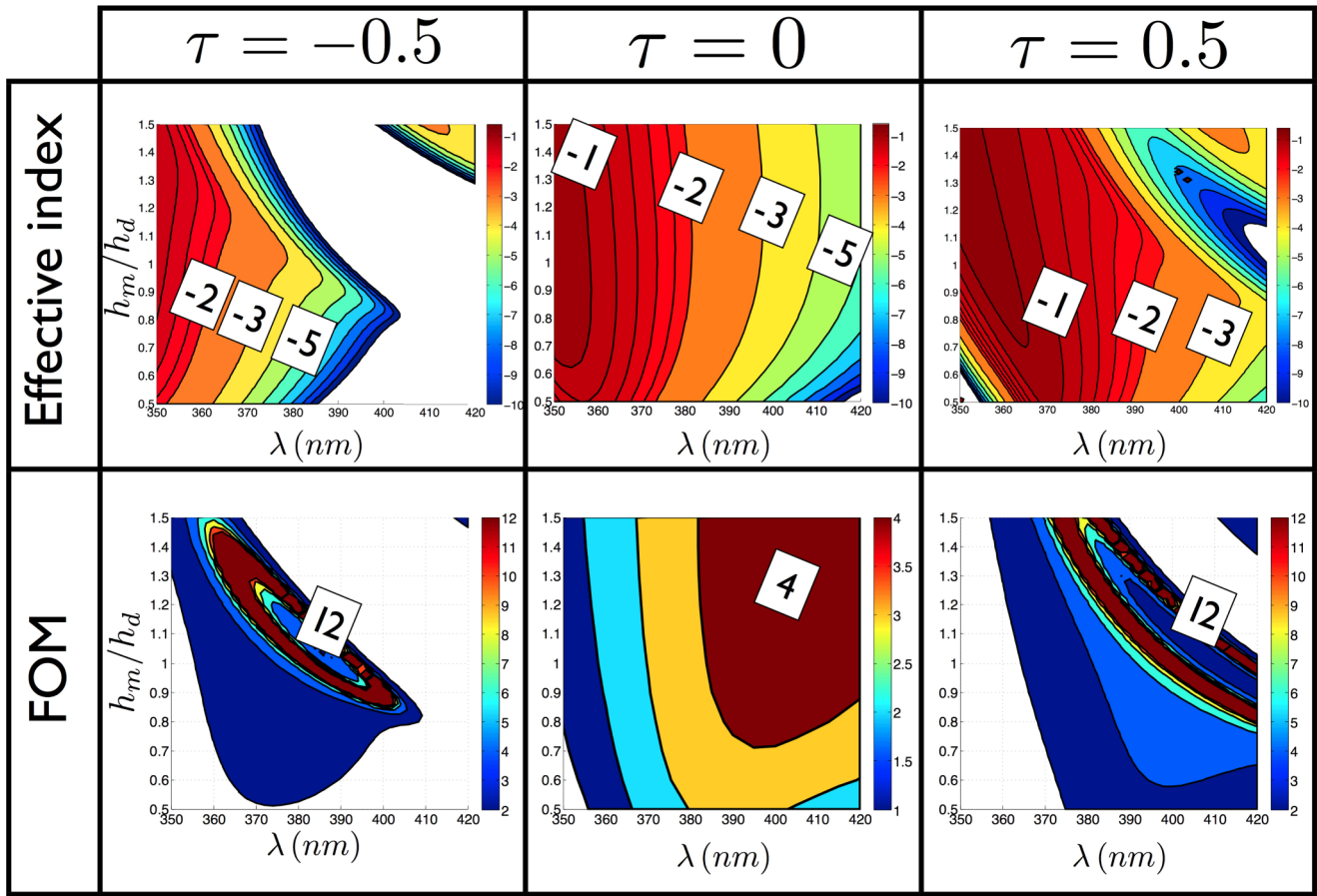
FIG. 6. (Color online) Maps of the effective index and FOM for three values of τ and as a function of the metal-dielectric ratio (h_m/h_d) and the wavelength. These results are obtained for the reduced frequency $D/\lambda = 0.16$ in the diffractive regime.

since the product of the wave vector (solid arrow) and the group velocity (dashed arrow) is always positive: $\mathbf{k} \cdot \mathbf{v}_g > 0$.

Using this approach, we are now able to study the modification of the effective index induced by the defect layer M_d in the diffractive regime for $D/\lambda = 0.16$. The effective index and the FOM computed from Eqs. (4) and (5) are plotted as functions of the wavelength, the ratio h_m/h_d, and for three values of τ (Fig. 6). Since in the diffractive regime the dispersion relations are very dependent on the lattice period, small variations of the (M_d) layer strongly modify the effective properties of the hyperbolic metamaterial. This behavior is observed for the isoindex curves calculated for $\tau = \pm 0.5$ that present complex shapes and rapid variations with both the wavelength and the metal-dielectric ratio. Even more importantly, the smooth variations of the FOM for the (MD) sequence (for $\tau = 0$) are replaced by sharper maps when the (M_d) layer is introduced. The FOM quadruples for some pairs of the metal-dielectric ratio and wavelength and attains large values of 12 for a negative effective index around -1.6. These results seem to be encouraging for achieving optimized flat lenses with superstructured HMs since a large FOM ensures a good transmission of evanescent waves through the multilayer. However, as demonstrated in the next section a large FOM is not sufficient to realize flat lenses making super-resolved images.

V. OPTICAL RESOLUTION OF FLAT LENSES BASED ON SUPERSTRUCTURED HYPERBOLIC METAMATERIALS

In the previous section we demonstrated that metallic defects enhance the transmission of waves of large wave vector throughout superstructured HMs when they operate in the diffractive regime. In this section, we add another parameter linked to the amount of waves that can be focalized by a lens and enable the diffraction limit to be surpassed. As shown by the following expression of the transmitted electromagnetic field through a HM, the transmission coefficient contains all the information about the optical efficiency of the lens [33,34]:

$$U(x,y) = \int_{-\infty}^{\infty} A(k_x)T(k_x)t_0(k_x,y)e^{ik_xx}dk_x. \quad (8)$$

In this Fourier integral, $t_0(k_x,y) = e^{iy\sqrt{k_0^2-k_x^2}}$ is the transfer function in the air medium and $A(k_x) = W_0/(2\sqrt{\pi}) \exp[-(k_x W/2)^2]$ is the spectrum of the incident Gaussian beam in k space. Because of the optical absorption, the transfer function of the multilayer has been proven to be well approximated by $T(k_x) = e^{i\bar{k}_y(k_x)L}$ since its spectrum is free of sharp resonances [21]. Here L is the total thickness of the lens and $\bar{k}_y$ represents the complex Bloch wave vector extracted from the dispersion relation of the infinite structure. Using the parabolic expansion of Eq. (3), the transmission
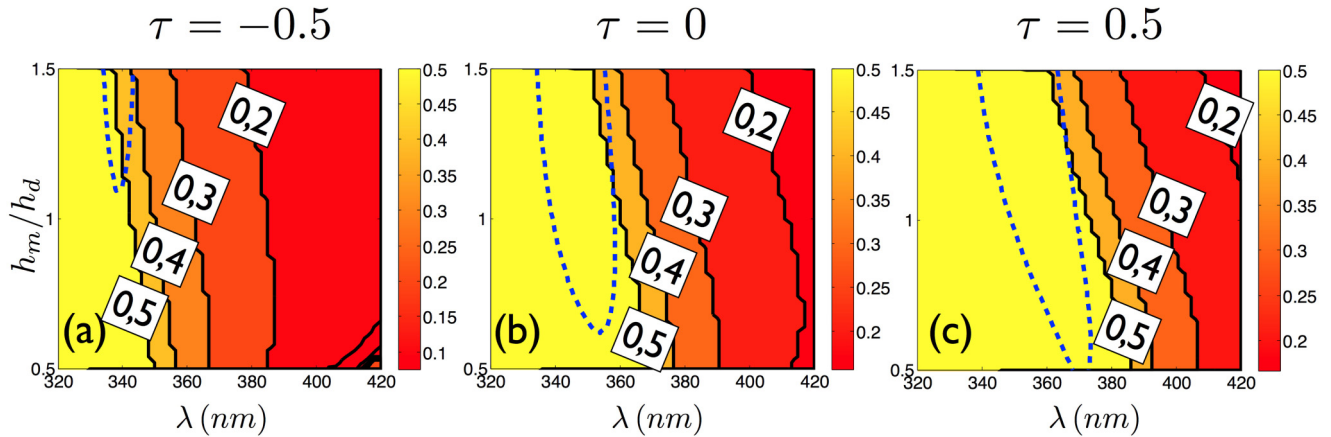
FIG. 7. (Color online) Maximal optical resolution in units of λ for three values of τ as a function of the metal-dielectric ratio (h_m/h_d) and the wavelength. The dashed curves are the -1 isoindex curves. These results are obtained for the reduced frequency $D/\lambda = 0.16$ in the diffractive regime.

coefficient is expressed in terms of the effective index n and of the FOM ($\mathcal{F}$):

$$T(k_x) = e^{i\bar{k}_y(0)L} e^{-k_x^2/2k_0 L/|n|\mathcal{F}} e^{-i(k_x^2/2k_0)(L/n)}. \quad (9)$$

The attenuation of the waves with high-k wave vector inside the lens is then driven by the FOM, which has to be as high as possible to provide a full reconstruction of the object in the image plane. However, a large FOM is not the sole condition for getting super-resolution. The Fourier transform of Eq. (10) is relevant under the assumption that the integral holds for very large transverse wave vector k_x. But, as seen on Fig. 5, in the diffractive regime, the IFCs present a finite-size extension in k space, which leads us to introduce a cutoff for the transverse wave vector named k_x^{cut}. Beyond this cut wave vector, no modes are allowed to propagate within the structure. One can estimate the maximal resolution, when a large FOM is assumed, by replacing the transmission coefficient by a top-hat function $T_p(kx) = 1$ for $|k_x| < k_x^{\text{cut}}$ and null otherwise. By substituting the transmission coefficient with $T_p(k_x)$ in Eq. (9) and for an image focalized close to the output interface, we obtain the following Fourier transform:

$$U(x,L) = \int_{-k_x^{\text{cut}}}^{k_x^{\text{cut}}} e^{ik_x x} dk_x, \quad (10)$$

which yields $U(x,L) = 2k_x^{\text{cut}}\text{sinc}(k_x^{\text{cut}}x)$. The full width at half maximum of the intensity profile $U^2(x,L)$ gives the maximal resolution $\Delta = \pi/k_x^{\text{cut}}$. To estimate the maximal resolution attainable for a flat lens made of HMs operating in the diffractive regime at $D/\lambda = 0.16$, we calculate Δ as a function of the wavelength and the filling ratio in metal; see Fig. 7. Since the effective index also varies with the thickness of the defect layer, the -1 isoindex curve is potted as a reference. For the (MD) multilayer, i.e., when $\tau = 0$, the maximal resolution cannot surpass $0.4/\lambda$ along this -1 isoindex curve. When the defect layer is added, for $\tau = 0.5$, the isoindex curve is redshifted, and the optical resolution of the flat lens is severely degraded. This behavior is amplified for larger metallic defect thicknesses. Very similar results are obtained for the flat lens studied in the experimental work of Xu and co-authors which correspond to $\tau = 1$. In that

case, the maximal resolution is close to $\lambda/2$ for $\lambda = 363$ nm and a metal-dielectric ratio $h_m/h_d = 1.14$. This demonstrates that, whatever the enhancement of the FOM provided by the metallic defect, the limiting parameter is clearly the maximal transverse wave vector k_x^{cut}. For the structure explored in [23], similar IFCs to those of Fig. 5(a) are obtained, with a shape that matches the air IFC. In that situation $k_x^{\text{cut}} = 2\pi/\lambda$ and thus the optical resolution $\Delta = \lambda/2$ cannot surpass the diffraction limit. The same conclusion applies for a thinner defect layer; when $\tau = -0.5$, both the -1 isoindex curve and the diffraction limit are blueshifted. Finally, in the diffractive regime, it is very difficult to find an operating point that presents simultaneously a large FOM and maximal optical resolution.

VI. DESIGN OF FLAT LENSES MADE OF SUPERSTRUCTURED HYPERBOLIC METAMATERIALS

In the previous section, we have shown that HMs scaled to work in the diffractive regime do not provide the required optical conditions to design a flat lens able to surpass the diffraction limit. The problem originates from the small transverse wave vectors attainable which limit the transmission of subwavelength optical information through the lens. In contrast, HM designs in the long-wavelength regime offer large IFCs that increase the optical resolution, but the metallic defect cannot enhance the FOM. In this section, we consider a regime between the homogenization and diffractive regimes in order to find an optimized structure that presents simultaneously a large FOM and a large cutoff wave vector. We consider the reduced frequency $D/\lambda = 0.11$ and explore the properties of three lenses presenting the same effective index but different FOMs and maximal resolutions Δ.

We start with an (MD) multilayer ($\tau = 0$) characterized by a maximal FOM $\mathcal{F} = 4$ for a blue radiation of 400 nm and for a metallic ratio $h_m/h_d = 1.4$. This lens (L_A), operating at the working point A on Figs. 8(a) and 8(b), presents an effective index of -5 and a maximal resolution $\Delta = 0.12\lambda$. We now introduce an (M_d) layer of thickness $h = 2h_m$ (i.e., for $\tau = 1$) into the HM. The -5 isoindex curve now presents a complex shape and a narrow region appears where the FOM attains very high values (typically larger than 20). We consider two
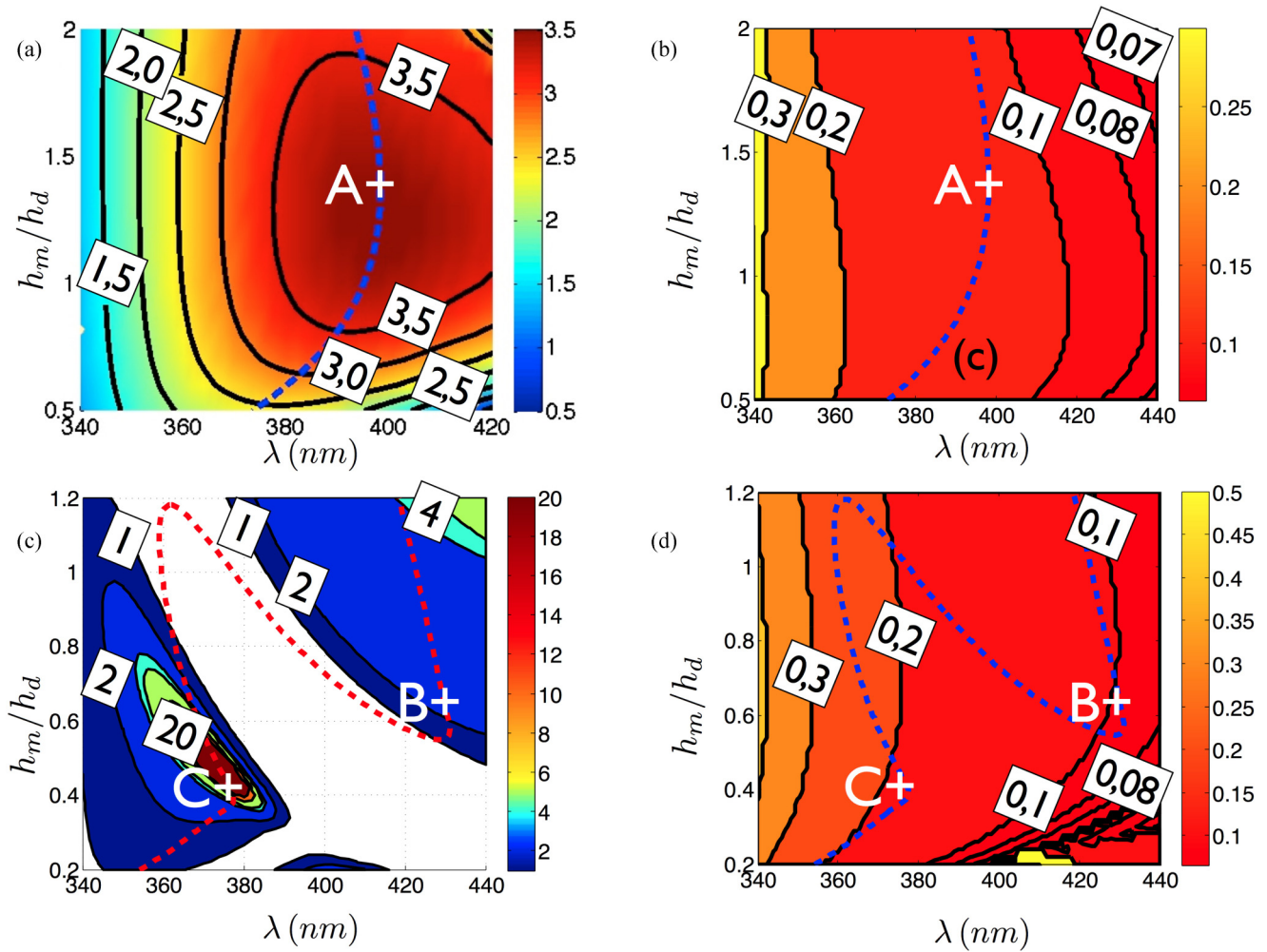
FIG. 8. (Color online) (a) and (b) Figure of merit (FOM) and resolution Δ for $\tau = 1$ and $D/\lambda = 0.11$. (c) and (d) Figure of merit and resolution for $\tau = 1$ and $D/\lambda = 0.11$. The dashed curves are the -5 isoindex curves.

working points B and C for a superstructured HM character-ized by the same -5 effective index but having different FOMs and maximal resolutions, Figs. 8(c) and 8(d). The lens (L_B) works at point B for a low FOM $\mathcal{F} = 2.4$ but a high resolution $\Delta = 0.1\lambda$ achieved at $\lambda = 430$ nm and for $h_m/h_d = 0.65$. The lens (L_C) operates at point C corresponding to a high FOM $\mathcal{F} = 28$ and a maximal optical resolution close to $\Delta = 0.2\lambda$ at $\lambda = 375$ nm and for $h_m/h_d = 0.45$.

To compare the optical efficiency of these three lenses, we simulate the propagation of a Gaussian beam of subwavelength waist (equal to $\lambda/100$) which is focalized at the input interface. The simulations are done with free software based on an exact modal method [35]. We also recall that, for a source located at the input interface of the lens, the position of the image satisfies the lens equation $f = -L/n$, where n represents the effective index defined by Eq. (4) [22]. Here, the total thickness L of the lens is varied to determine the optical resolution as a function of the focal distance f. The full width at half maximum of the focalized beam is then recorded at f (Fig. 9). The lens (L_A) is seen to focalize with a subwavelength resolution until the focal distance reaches 0.8λ, a result in agreement with [21]. The lens (L_B) shows worse optical performance with an optical resolution larger than Abbe's limit for a focal distance upper than $\lambda/2$. This result highlights the fact that, despite

the high maximal resolution of $\lambda/10$, the low FOM of 2.4 hinders the high-k waves from propagating efficiently through
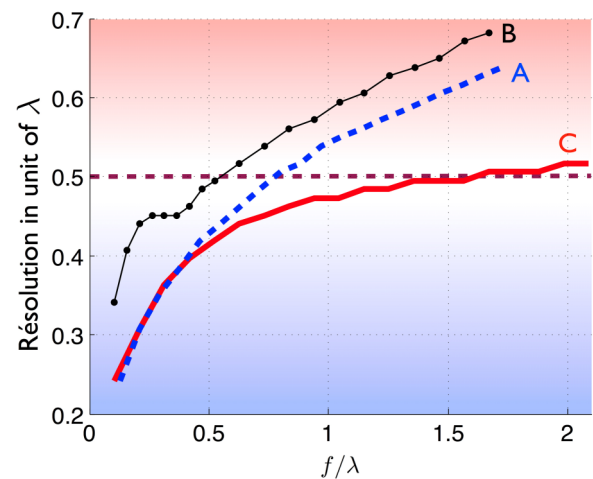
FIG. 9. (Color online) Optical resolution with respect to the focal distance expressed in units of wavelength for the three flat lenses. The dashed curve corresponds to lens (L_A) based on an (MD) sequence. The solid and dotted curves correspond respectively to lenses (L_C) and (L_B) based on a superstructured HMs.

the lens, which severely degrades the optical resolution. The lens (L_C) demonstrates the best optical performances since subwavelength resolution occurs for a focal distance as large as $f = 1.9\lambda$. Moreover, the high FOM $\mathcal{F} = 28$ of lens L_C enables an image to be focused in the vicinity of the outgoing edge of the lens (for $f = 0.2\lambda$) with an optical resolution of 0.24λ very close to the maximal optical resolution $\Delta = 0.2\lambda$. This again highlights the positive impact of a high FOM in getting an optimal resolution.

VII. CONCLUSION

We have demonstrated that superstructured HMs that integrate periodic metallic defects have a modified effective permittivity tensor. These variations are quantified through the calculation of an effective index and the associated figure of merit. For HMs that are designed to work in the homogenization regime, this superstructuring is shown to have a modest impact on the optical properties. In contrast, in the diffractive regime, the effective losses are very greatly decreased by the additional metallic defect layers for appropriate choices of the metal-dielectric ratio and wavelength. Additionally, the superstructuring provides an efficient way to realize HMs of -1 effective optical indices operating in the visible spectrum of light. However, the reduced extension of the dispersion curve in k space is demonstrated to definitely prevent subwavelength focusing. In the diffractive regime, a cutoff hinders propagation of waves with a very high transverse wave vector, so that they are not channeled through the HM. This explains the experimental results obtained in [24], where the super-resolution is totally absent. In order to reach super-resolution, HMs must be optimized both in terms of absorption losses (i.e., they must reach a high figure of merit) and in terms of the transverse-wave vector cutoff. Finally, we have demonstrated that large FOMs associated with high optical resolution are obtained with optimized structures designed to work in an intermediate regime between the homogenization and diffractive regimes. Based on that finding, electromagnetic simulations show that these superstructured HMs provide super-resolved visible images (at 375 nm) and for large focal distances up to 2λ. These tools provide the method for producing optimized HMs and open several questions as to why such enhanced optical properties emerge.

[1] D. R. Smith and D. Schurig, Phys. Rev. Lett. **90**, 077405 (2003).

[2] A. Poddubny, I. Iorsh, P. Belov and Y. Kivshar, Nat. Photonics **7**, 948 (2013).

[3] V. P. Drachev, V. A. Podolskiy, and A. V. Kildishev, Opt. Express **21**, 15048 (2013).

[4] D. Lu, J. J. Kan, E. E. Fullerton, and Z. Liu, Nat. Nanotechnol. **9**, 48 (2014).

[5] J. Kim, V. P. Drachev, Z. Jacob, G. V. Naik, A. Boltasseva, E. E. Narimanov, and V. M. Shalaev, Opt. Express **20**, 8100 (2012).

[6] W. D. Newman, C. L. Cortes, and Z. Jacob, J. Opt. Soc. Am. B **30**, 766 (2013).

[7] Y. Guo, S. Molesky, H. Hu, C. L. Cortes, and Z. Jacob, Appl. Phys. Lett. **105**, 073903 (2014).

[8] D. Ji, H. Song, X. Zeng, H. Hu, K. Liu, N. Zhang, and Q. Gan, Sci. Rep. **4**, 4498 (2014).

[9] I. S. Nefedov, C. A. Valagiannopoulos, S. M. Hashemi, and E. I. Nefedov, Sci. Rep. **3**, 2662 (2013).

[10] J. Liu, G. V. Naik, S. Ishii, C. DeVault, A. Boltasseva, V. M. Shalaev, and E. Narimanov, Opt. Express **22**, 8893 (2014).

[11] Y. Guo and Z. Jacob, Opt. Express **21**, 15014 (2013).

[12] S. A. Biehs, M. Tschikin, and P. Ben-Abdallah, Phys. Rev. Lett. **109**, 104301 (2012).

[13] P. A. Belov, C. R. Simovski, and P. Ikonen, Phys. Rev. B **71**, 193105 (2005).

[14] P. A. Belov and Y. Hao, Phys. Rev. B **73**, 113110 (2006).

[15] H. Shin and S. Fan, Appl. Phys. Lett. **89**, 151102 (2006).

[16] Y. Jin, Prog. Electromagn. Res. **105**, 347 (2010).

[17] W. Yan, N. Asger Mortensen, and M. Wubs, Opt. Express **21**, 15026 (2013).

[18] K. G. Balmain, A. A. E. Luttgen, and P. C. Kremer, IEEE Antennas Wireless Propag. Lett. **1**, 146 (2002).

[19] G. V. Eleftheriades and O. F. Siddiqui, IEEE Trans. Microwave Theory Tech. **53**, 396 (2005).

[20] S. H. Sedighy, C. Guclu, S. Campione, M. M. Amirhosseini, and F. Capolino, IEEE Trans. Microwave Theory Tech. **61**, 4110 (2013).

[21] J. Benedicto, E. Centeno, R. Pollès, and A. Moreau, Phys. Rev. B **88**, 245138 (2013).

[22] J. Benedicto, E. Centeno, and A. Moreau, Opt. Lett. **37**, 4786 (2012).

[23] E. Verhagen, R. de Waele, L. Kuipers, and A. Polman, Phys. Rev. Lett. **105**, 223901 (2010).

[24] T. Xu, A. Agrawal, M. Abashin, K. J. Chau, and H. J. Lezec, Nature (London) **497**, 470 (2013).

[25] E. E. Narimanov, Phys. Rev. X **4**, 041014 (2014).

[26] E. D. Palik, *Handbook of Optical Constants of Solids* (Academic, New York, 1991).

[27] X.-B. Kang, W. Tan, and Z.-G. Wang, Opt. Commun. **284**, 4237 (2011).

[28] O. Kidwai, S. V. Zhukovsky, and J. E. Sipe, Opt. Lett. **36**, 2530 (2011).

[29] C. Guclu, S. Campione, and F. Capolino, Phys. Rev. B **86**, 205130 (2012).

[30] O. Kidwai, S. V. Zhukovsky, and J. E. Sipe, Phys. Rev. A **85**, 053842 (2012).

[31] A. Andryieuski, A. V. Lavrinenko, and S. V. Zhukovsky, Nanotechnology **26**, 184001 (2015).

[32] R. Maas, E. Verhagen, J. Parsons, and A. Polman, ACS Photonics **1**, 670 (2014).

[33] N. Mattiucci, G. Daguanno, M. Scalora, M. J. Bloemer, and C. Sibilia, Opt. Express **17**, 17517 (2009).

[34] B. Wood, J. B. Pendry, and D. P. Tsai, Phys. Rev. B **74**, 115116 (2006).

[35] F. Krayzel, R. Pollès, A. Moreau, M. Mihailovic, and G. Granet, J. Eur. Opt. Soc.: Rap. Pub. **5**, 10025 (2010).